International Dairy Journal 118 (2021) 105023

Contents lists available at ScienceDirect

International Dairy Journal

journal homepage: www.elsevier.com/locate/idairyj

Temperature effects on spontaneous supersaturation of calcium citrate in presence of lactate

Xiao-Chen Liu, Jacob J.K. Kirkensgaard, Leif H. Skibsted*

Department of Food Science, University of Copenhagen, Rolighedsvej 26, DK-1958 Frederiksberg C, Denmark

ARTICLE INFO

Article history:
Received 3 November 2020
Received in revised form
31 January 2021
Accepted 31 January 2021
Available online 13 February 2021

ABSTRACT

Supersaturation of calcium salts of low solubility is important for biomineralisation. The dynamics of solutions supersaturated in calcium citrate prepared by dissolving calcium lactate and sodium citrate in water, serving as a mineralisation model, were characterised electrochemically and by small-angle X-ray scattering. The process was divided into: (i) citrate assisted dissolution of calcium lactate with an enthalpy of activation of 115 kJ mol^{-1}; (ii) a metastable homogeneous supersaturation phase, where calcium ion activity continues to increase despite constant calcium concentration; (iii) calcium ion activity decreasing with an enthalpy of activation of 30 kJ mol^{-1} together with 3-dimensional crystallisation with an enthalpy of activation of 177 kJ mol^{-1}. The differences in activation enthalpies lead to a higher degree of supersaturation at higher temperatures but longer lasting supersaturation at low temperature as was seen for critical supersaturation of up to a factor of 20 resulting in non-linear temperature effects for calcium mobility.

1. Introduction

Biological fluids involved in tissue mineralisation in mammals are supersaturated in calcium phosphates like octacalcium phosphate and hydroxyapatite. Controlled precipitation in hard tissue but not in soft tissue is crucial for maintaining bone strength and simultaneously for prevention of vascular calcification, otherwise leading to serious pathogenic conditions (Holt, 2013; Holt, Sorensen, & Clegg, 2009; Li, Wang, & Putnis, 2017; Wang & Ma, 2020). The dynamics of growth of mineral tissue in teeth and bone is increasingly becoming understood based on thermodynamic descriptions of calcium phosphate clusters of various structure (Bijl, Huppertz, van Valenberg, & Holt, 2019; Quarto et al., 2018; Wang, Ma, & Liu, 2009; Zhou, Xue, & Yang, 2013).

The dynamics of formation of the supersaturated biological fluids including milk has been far less investigated. However, it appears that citrate plays a key role in the mobility of calcium in mammals and their milk and in creating supersaturation at ambient temperature. Citrate is thus important for stabilisation of calcium in the serum phase of milk from different mammals despite the very low aqueous solubility of calcium citrate (Gueguen & Pointillart, 2000; Vavrusova & Skibsted, 2016). Calcium citrate has moreover been found to promote regeneration of damaged bones in animals under conditions of experimental surgery (Wang et al., 2012). Recently, a metabolomics analysis has identified a positive correlation between the level of circulating citrate in humans and mineral turnover important for maintenance of bone strength (Hartley et al., 2020), findings which highlight the importance of milk as an important nutrient.

A unique role of citrate in increasing bioavailability of calcium from dietary supplements has also long been documented (Kaduk, 2018). Excess citrate was even demonstrated to increase calcium absorption from calcium citrate in human intervention studies (Holt, Lenton, Nylander, Sorensen, & Teixeira, 2014; Pak, Harvey, & Hsu, 1987). The effect of excess citrate seems to relate to the capability of hydroxycarboxylates like citrate spontaneously to establish solutions strongly supersaturated in calcium hydroxycarboxylates (Vavrusova, Danielsen, Garcia, & Skibsted, 2018; Vavrusova, Garcia, Danielsen, & Skibsted, 2017). For the combination of calcium lactate and sodium citrate, supersaturation of a factor of more than 20 for calcium citrate was seen at ambient temperature conditions. The tendency for formation of supersaturation for calcium salt was concluded to be inversely correlated with the association constants of calcium complexes of the hydroxycarboxylates: lactate > gluconate > citrate (Vavrusova et al., 2017).

The combination of calcium lactate and sodium citrate was accordingly selected for the study of kinetics behind the spontaneous supersaturation and the factors determining the degree of

* Corresponding author. Tel.: +45 3533 3221.
E-mail address: ls@food.ku.dk (L.H. Skibsted).

https://doi.org/10.1016/j.idairyj.2021.105023
0958-6946/

supersaturation and the robustness of supersaturation, including the effect of temperature using a combination of electrochemical methods and small-angle X-ray scattering (SAXS) to follow the phase transitions.

2. Materials and methods

2.1. Chemicals

Calcium L-lactate pentahydrate ($CaLact_2 \cdot 5H_2O$, CLP), sodium citrate dihydrate ($Na_3Citr \cdot 2H_2O$, NCD), calcium citrate tetrahydrate ($Ca_3Citr_2 \cdot 4H_2O$, CCT), calcium chloride dihydrate ($CaCl_2 \cdot 2H_2O$) were purchased from Sigma Aldrich (Steinheim, Germany). Water deionised by a Milli-Q Plus unit (Millipore Corp., Bedford, MA, USA) was used throughout. Calcium citrate hexahydrate ($Ca_3Citr_2 \cdot 6H_2O$, CCH) was made by mixing an equal volume of NCD (0.030 M) and $CaCl_2$ (0.045 M) solutions, and collecting the formed precipitate after 24 h at room temperature, after which the precipitate was washed with water followed by ethanol, and dried at 25 °C for 3 days (Chatterjee & Dhar, 1924).

2.2. Dissolution experiment

Different amounts of CLP and NCD were used to determine the critical ratio between the two compounds for critical supersaturation of calcium citrate by a trial and error method at 15, 25, 37 °C. 100 mL water was added to known amount of CLP and NCD, which were dissolved with constant stirring. Dissolution was confirmed if the solution became clear and without particles in two hours. The combination of CLD and NCD are shown in Fig. 1, marked as homogeneously supersaturated solutions without particles, as inhomogeneously supersaturated solutions with excess of solid CLP, or at the borderline as critically supersaturated solutions. The critically supersaturated solutions were accordingly clear solutions, which could not dissolve any further calcium lactate solids.

2.3. Small-angle X-ray scattering (SAXS)

Small-angle X-ray scattering (SAXS) is a diffraction method which can be used to follow the process of crystal formation in solution. Supersaturated solutions were made by adding 100 mL water to a mixture of 0.0519 mol CLP and 0.0408 mol NCD at 25 °C and crystallisation from the supersaturated solution was followed by SAXS at 15, 25, and 37 °C. SAXS measurements were performed using a GANESHA instrument from SAXSLAB (Lyngby, Denmark) with a Rigaku (Rigaku-Denki, Co., Tokyo, Japan) 40 W micro-focused Cu-source producing X-rays and a wavelength of $\lambda = 0.154$ nm detected by a moveable Pilatus 300k pixel-detector from Dectris (Baden, Switzerland) allowing different length scales to be measured. The two-dimensional scattering data were azimuthally averaged and corrected for detector inhomogeneities using standard reduction software (SAXSGUI, Lyngby, Denmark). The radially averaged intensity (*Int.*) from the detector is given as a curve against the scattering vector $q = 4\pi \cdot \sin\theta/\lambda$, where λ is the wavelength, and 2θ is the scattering angle as previously described (Liu, Kirkensgaard, & Skibsted, 2021). The intensity of the crystallisation process was followed at $q = 0.036$ nm, as shown in Figs. 2 and 6.

2.4. Calcium ion activity measurement

A selective electrode ISE25Ca for calcium ions and a reference electrode REF251 were from Radiometer (Copenhagen, Denmark) and used to measure the activity of calcium ion $a(Ca^{2+})$. The standards were $CaCl_2$ aqueous solutions with concentrations of 1.00×10^{-4}, 1.00×10^{-3}, and 1.00×10^{-2} M for calibration at varying temperatures (Righellato & Davies, 1930). $a(Ca^{2+})$ in the standards were calculated according to Eq. (1),

$$a(X^{z\pm}) = \gamma^{z\pm} \cdot [X^{z\pm}] \quad (1)$$

where $a(X^{z\pm})$ is the activity of ion $X^{z\pm}$, and $[X^{z\pm}]$ is the concentration of $X^{z\pm}$. $\gamma^{z\pm}$ is the coefficient of activity of ion $X^{z\pm}$ calculated from extended Debye–Hückel equation (Eq. (2)),

$$\log_{10} \gamma^{z\pm} = -A_{DH} z^2 \left(\sqrt{I} / (1+\sqrt{I}) - nI\right) \quad (2)$$

where A_{DH} is the Debye–Hückel constants of 0.501, 0.510, and 0.522 at 15, 25, and 37 °C, respectively, and z is the charge of the ions. e.g. $z = 2$ for Ca^{2+}, n equals 0.3 is selected for these conditions (Davies, 1962). I is the ionic strength of the aqueous solution as calculated by Eq. (3),

$$I = 0.5 \sum (z^2 [X^{z\pm}]) \quad (3)$$

2.5. Temperature effect on supersaturation

Supersaturation and precipitation from supersaturated solution resulting from dissolution of NCD and CLP were followed by SAXS and calcium ion activity measurement at 15, 25, 37 °C.

2.6. Speciation of supersaturated solutions

The reactions CLP and NCD during dissolution, metastable supersaturation, and precipitation include:

$$CaLact_2 \cdot 5H_2O \rightleftharpoons Ca^{2+} + 2Lact^- + 5H_2O \quad (4)$$

$$Na_3Citr \cdot 2H_2O \rightleftharpoons 3Na^+ + Citr^{3-} + 2H_2O \quad (5)$$

$$3Ca^{2+} + 2Citr^{3-} + 6H_2O \rightleftharpoons Ca_3Citr_2 \cdot 6H_2O\,(s) \quad (6)$$

together with the association processes for complexes ($K_{ass,c}$ is association constants based on concentrations) for unity ionic strength (Vavrusova, Liang, & Skibsted, 2014; Vavrusova & Skibsted, 2016),

$$Ca^{2+} + Lact^- \rightleftharpoons CaLact^+, \quad K_{ass,c}(25^\circ\ C) = 8\ M^{-1} \quad (7)$$

$$Ca^{2+} + Citr^{3-} \rightleftharpoons CaCitr^-, \quad K_{ass,c}(25^\circ\ C) = 2400\ M^{-1} \quad (8)$$

and the dissociation of citric acid and water ($K_{diss,c}$ is dissociation constants based on concentrations) (Apelblat & Barthel, 1991),

$$H_3Citr \rightleftharpoons H^+ + H_2Citr^-, \quad K_{diss,c}(25^\circ\ C) = 6.98 \times 10^{-4}\ M \quad (9)$$

$$H_2Citr^- \rightleftharpoons H^+ + HCitr^{2-}, \quad K_{diss,c}(25^\circ\ C) = 1.40 \times 10^{-5}\ M \quad (10)$$

$$HCitr^{2-} \rightleftharpoons H^+ + Citr^{3-}, \quad K_{diss,c}(25^\circ\ C) = 4.05 \times 10^{-7}\ M \quad (11)$$

$$H_2O \rightleftharpoons H^+ + OH^-, \quad K_{diss,c}(25^\circ\ C) = 1.01 \times 10^{-14}\ M^2 \quad (12)$$

The species in solution meet the mass balance and electroneutrality principles which for condition with 0.519 mol CLP and 0.408 mol NCD in 1000 mL water with a density of 1.16 g mL^{-1} at 25 °C yield:

$$[\text{Lact}]_{\text{total}} = [\text{CaLact}^+] + [\text{Lact}^-] = 2\,([\text{Ca}^{2+}] + [\text{CaCitr}^-] + [\text{CaLact}^+]) \quad (13)$$

during dissolution, with a value of 0.937 M during metastable supersaturation and precipitation.

$$[\text{Na}]_{\text{total}} = 3[\text{Na}_3\text{Citr}\cdot 2\text{H}_2\text{O}]_{\text{added}} = 1.10\ \text{M} \quad (14)$$

$$[\text{H}^+] + [\text{Na}^+] + 2[\text{Ca}^{2+}] + [\text{CaLact}^+] = [\text{OH}^-] + [\text{H}_2\text{Citr}^-] + 2[\text{HCitr}^{2-}] + 3[\text{Citr}^{3-}] + [\text{CaCitr}^-] + [\text{Lact}^-] \quad (15)$$

$a(\text{Ca}^{2+}) = \gamma^{2+}_{\text{Ca}}\cdot[\text{Ca}^{2+}]$ and $a(\text{H}^+) = \gamma^{+}_{\text{H}}\cdot[\text{H}^+]$ measured electrochemically were used to calculate speciation in supersaturated solutions by combining Eq. (1) and Eqs. (7)–(15). I was assumed to be around unity and γ for Ca^{2+} around 0.30 was accordingly used for calculations, as discussed below.

2.7. Differential scanning calorimeter

A total of about 10 mg samples were used for differential scanning calorimeter (DSC) measurements by a DSC STAR^e System from Mettler Toledo (Schwerzenbach, Switzerland) (Cheng, Garcia, Tang, Danielsen, & Skibsted, 2018). The measurements were performed from 25 to 200 °C with a scanning rate of 10 °C min^{-1}.

2.8. Density functional theory calculation

Gaussian 09 software was used to optimise the structures of monomer and dimer of the calcium citrate complex in aqueous solution based on B3LYP method at 6–311g++ (d, p) level combined with the solvent mode of integral equation formalism variant (IEFPCM) (Frisch et al., 2009). The thermodynamic parameters for optimised structures were used for calculating the changes of enthalpy (ΔH^0), entropy (ΔS^0) and free energy (ΔG^0) during the dimerisation reaction.

3. Results

Aqueous solubility of calcium lactate was found to increase dramatically in the presence of sodium citrate. In a series of trial and error experiments varying amounts of calcium lactate pentahydrate (CLP) were added to water together with varying amounts of sodium citrate dihydrate (NCD) under constant stirring. The dissolution process was followed for 2 h at which time the reaction mixture was classified as homogeneous or inhomogeneous by visual inspection (Vavrusova et al., 2017). All combinations of CLP and NCD investigated resulted in concentrations of calcium and citrate strongly exceeding the equilibrium solubility of calcium citrate. The homogeneous solutions were accordingly to a varying degree all supersaturated in calcium citrate but with the capability of increasing the calcium citrate concentration by continuing the dissolution process. The inhomogeneous reaction mixtures were also supersaturated but without the capability of increasing the calcium citrate concentration through continuing the dissolution process. By trial and error, the combinations of CLP and NCD providing the critical conditions at the borderline between the inhomogeneous and homogeneous reaction mixtures were identified at each of the three temperatures of 15, 25 and 37 °C. The critical conditions correspond to combinations of CLP and NCD being supersaturated in Ca_3Citr_2 and without the capability of increasing the supersaturation by continuing dissolution. The critical conditions were found to be accounted for by a linear relation between the applied amount of NCD and the dissolved CLP.

To study the temperature effect on the critical conditions for supersaturation, the combinations of CLP + NCD were investigated at

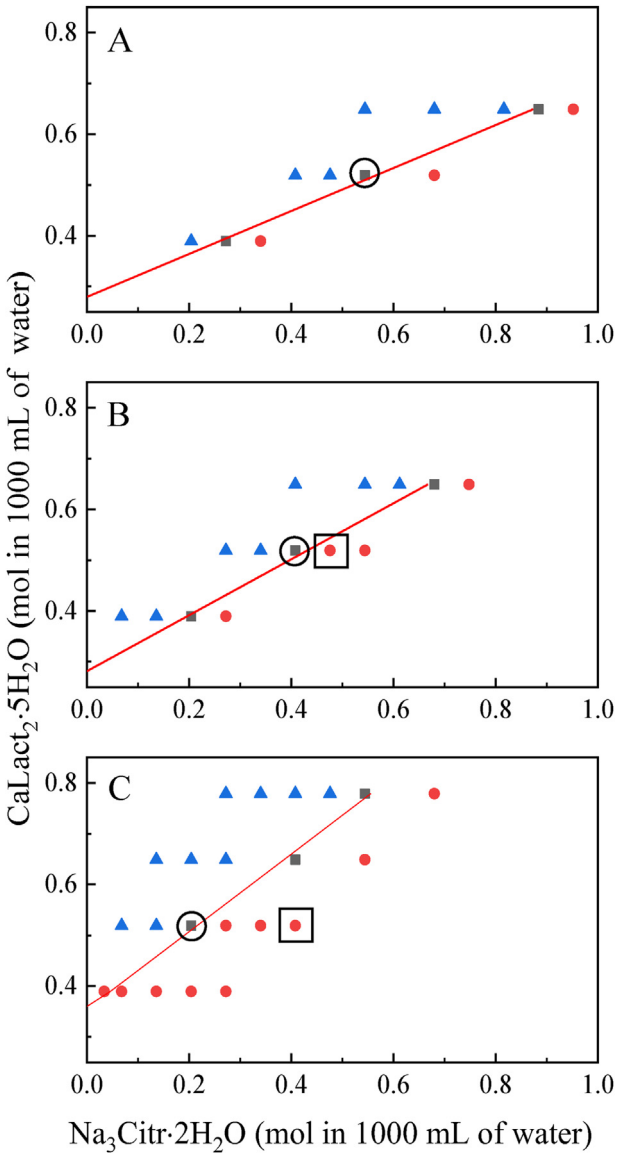

Fig. 1. Combination of $CaLact_2\cdot 5H_2O$ and $Na_3Citr\cdot 2H_2O$ for spontaneous formation of supersaturated solution as found by visual inspection at (A) 15, (B) 25, and (C) 37 °C: ●, and ▲ indicate formation of homogeneous supersaturated solutions and inhomogeneous supersaturated solutions, respectively, while ■ indicates combinations for critical spontaneous supersaturation. The points with squares or circles are the conditions selected for kinetics studies of changes in calcium ion activity as shown in Fig. 7.

15, 25, 37 °C as shown in Fig. 1. The critical conditions confirm that the smallest amounts of NCD needed for dissolution of CLP were different for the same amount of CLP at different temperatures. For each temperature, the relationship between the concentrations of CLP and NCD found to establish the critical conditions shows the following linear relationships at 15, 25 and 37 °C:

$$c_{\text{CLP}} = (0.422 \pm 0.027) \times c_{\text{NCD}} + (0.28 \pm 0.02) \quad (16)$$

$$c_{\text{CLP}} = (0.542 \pm 0.045) \times c_{\text{NCD}} + (0.29 \pm 0.02) \quad (17)$$

$$c_{\text{CLP}} = (0.753 \pm 0.087) \times c_{\text{NCD}} + (0.36 \pm 0.04) \quad (18)$$

The slopes found and presented with standard deviation from linear regression were 0.422, 0.542, and 0.753 for 15, 25, 37 °C, respectively, indicating that 1 mol NCD assists in dissolving 0.422,

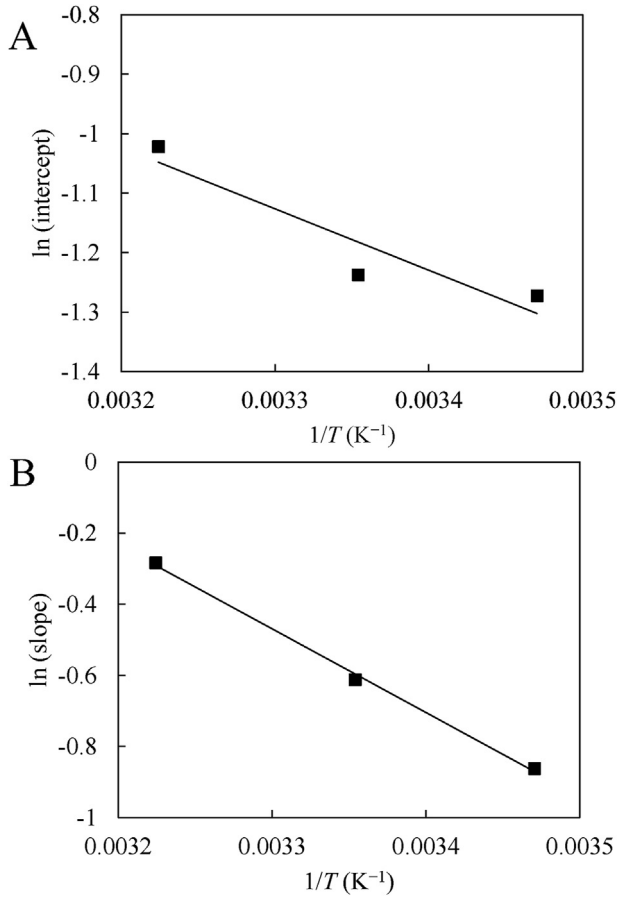

Fig. 2. Relationship between intercept or slope and temperature from temperature dependence of solubility of $CaLact_2 \cdot 5H_2O$ in water as extrapolated from solubility in presence of $Na_3Citr \cdot 2H_2O$ (A), and (B) stoechiometric factor for critical conditions for formation of supersaturated solutions of $CaLact_2 \cdot 5H_2O$ and $Na_3Citr \cdot 2H_2O$ codissolved in water, as shown in Eqs. (16)–(18). From linear regression, $\Delta H^0 = 8.6 \pm 3.3$ kJ mol^{-1} and $\Delta H^0 = 19.6 \pm 0.9$ kJ mol^{-1} is calculated for the citrate non-assisted and assisted dissolution, see Fig. 1, together with $\Delta S^0 = 19 \pm 7$ J·mol^{-1} K^{-1} and $\Delta S^0 = 61 \pm 3$ J mol^{-1} K^{-1} according to the van't Hoff equation.

0.542, and 0.753 mol CLP in the NCD concentration range investigated in addition to equilibrium solubility of CLP in water. The intercepts of the linear relationship increases with temperature according to 0.28 (15 °C) < 0.29 (25 °C) < 0.36 (37 °C) mol of CLP in 1000 mL water which can be compared with the CLP solubilities of 0.144, 0.206, and 0.343 mol/L^{-1} in water at 15, 25, and 37 °C (Kubantseva & Hartel, 2002). The enthalpy of dissolution of CLP in water and the enthalpy of citrate assisted dissolution of CLP were estimated using the van't Hoff equation (Eq. (19)) providing the positive enthalpies of dissolution of 9 and 20 kJ·mol^{-1}, respectively, as shown in Fig. 2.

Table 1
The lag phase (*LP*) and rate constant k_B based on a Boltzmann distribution model and rate constant k_A.[a]

Parameter	*LP* (h)	k_B (h^{-1})	k_A (h^{-1})
15 °C	2.22	1.32	0.010
25 °C	1.14	3.74	0.074
37 °C	0.59	9.88	2.014
$\Delta H^{\#}$ (kJ mol^{-1})	−47.4 ± 1.6	65.6 ± 3.4	177 ± 20
$\Delta S^{\#}$ (J mol^{-1} K^{-1})	−402 ± 14	−14.5 ± 0.7	331 ± 36

[a] Based on an Avrami model from SAXS measurement of crystallisation of $Ca_3Citr_2 \cdot 6H_2O$ from solutions of $CaLact_2 \cdot 5H_2O$ (CLP, 0.519 mol) and $Na_3Citr \cdot 2H_2O$ (NCD, 0.408 mol) in 1000 mL water as shown in Fig. 6.

$$\ln(\text{Intercept}) \text{ or } \ln(\text{Slope}) = -\Delta H^0_{\text{dissol}}/R \cdot 1/T + \Delta S^0_{\text{dissol}}/R \quad (19)$$

where $\Delta H^0_{\text{dissol}}$ is enthalpy of dissolution, and $\Delta S^0_{\text{dissol}}$ is entropy of dissolution. Both dissolution of CLP in water and the citrate assisted dissolution for 1 mol/L^{-1} of citrate are endothermic processes, for the CLP dissolution in agreement with previous findings (Kubantseva & Hartel, 2002).

Following the dissolution of CLP in presence of NCD the strongly supersaturated solutions stayed homogeneous for a varying period of time depending on degree of supersaturation and on temperature, see Table 1. To follow the dissolution process and changes in speciation during the metastable supersaturation period and during precipitation of calcium citrate, electrochemical measurement of calcium ion activity was combined with measurement of solid formation using SAXS. The calcium activity and the intensity at $q = 0.036$ nm for crystal nucleation and growth during the three phases are shown in Fig. 3 for all three temperatures of 15, 25 and 37 °C for 0.519 mol CLP and 0.408 mol NCD in 1000 mL of water, corresponding to one set of critical conditions at 25 °C as seen from Fig. 1. The SAXS dynamics shown as intensity/time curves in Fig. 3B showed an increase in the final intensity level according to 25 °C > 37 °C > 15 °C corresponding to a more significant formation of crystals at 25 °C. In agreement with this temperature dependence of crystallisation from the supersaturated solution, the lowest calcium ion activity was seen for 25 °C during the metastable supersaturation phase (Fig. 3A). The speciation of the solution during the three phases (dissolution, metastable supersaturation, precipitation) is shown in Table 2 for 25 °C.

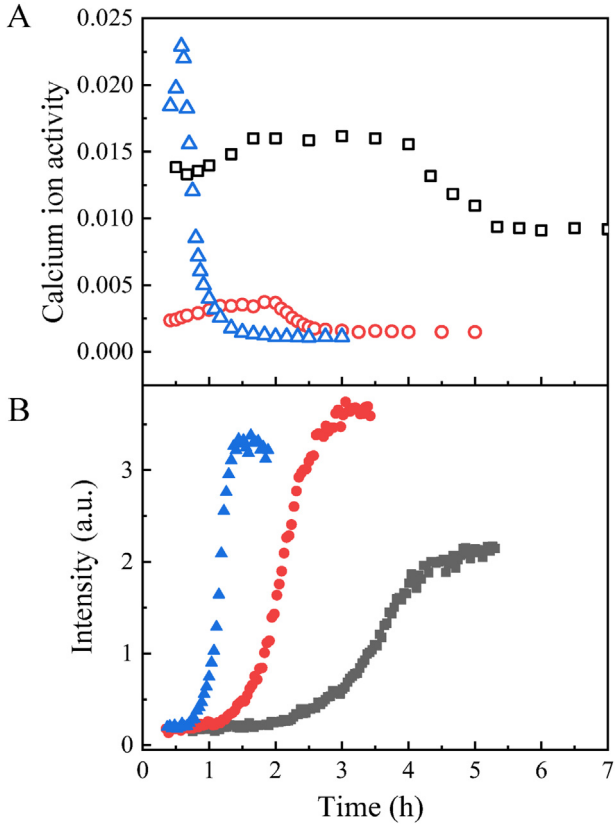

Fig. 3. Calcium activity (A; open symbols) as measured electrochemically following dissolution at 25 °C of $CaLact_2 \cdot 5H_2O$ (0.519 mol) + $Na_3Citr \cdot 2H_2O$ (0.408 mol) in 1000 mL water and precipitation of $Ca_3Citr_2 \cdot 6H_2O$ from the supersaturated solution and (B; closed symbols) scattering intensity from SAXS measurement during the precipitation process at 15 °C (□,■), 25 °C (○,●), and 37 °C (△,▲).

Table 2
Calculated speciation (in M) based on electrochemical measurement (calcium ion activity and pH) during codissolution, metastable supersaturation and precipitation for the critical condition for spontaneous supersaturation of 0.519 mol $CaLact_2 \cdot 5H_2O$ and 0.408 mol $Na_3Citr \cdot 2H_2O$ in 1000 mL water at 25 °C.[a]

Time (h)	$[Ca]_{total}$	$a(Ca^{2+})$	$[Ca^{2+}]$	$[CaLact^+]$	$[CaCitr^-]$	$[Na^+]$	$[Lact^-]$	$[H_3Citr]$	$[H_2Citr^-]$	$[HCitr^{2-}]$	$[Citr^{3-}]$	$[H^+]$	I	Q ($CaLact_2$)	Q (Ca_3Citr_2)	$[Ca^{2+}]*[CaCitr^-]^2$	Q/K_{sp} ($CaLact_2$)	Q/K_{sp} (Ca_3Citr_2)
Two phases during dissolution																		
0.02	0.358	0.00151	0.0038	0.0210	0.333	1.10	0.695	3.20E-10	7.07E-06	3.13E-03	0.0401	3.16E-08	1.27	1.82E-03	8.65E-11	4.19E-04	0.31	4.80E+05
0.03	0.369	0.00176	0.0044	0.0251	0.340	1.10	0.713	2.81E-10	6.19E-06	2.74E-03	0.0351	3.16E-08	1.26	2.23E-03	1.05E-10	5.07E-04	0.39	5.82E+05
0.07	0.371	0.00181	0.0045	0.0259	0.340	1.10	0.716	4.44E-10	8.34E-06	3.14E-03	0.0343	3.72E-08	1.26	2.31E-03	1.08E-10	5.23E-04	0.40	6.01E+05
0.10	0.378	0.00199	0.0050	0.0290	0.344	1.10	0.728	4.07E-10	7.65E-06	2.88E-03	0.0314	3.72E-08	1.26	2.64E-03	1.22E-10	5.91E-04	0.46	6.79E+05
0.17	0.383	0.00210	0.0053	0.0309	0.347	1.10	0.734	5.12E-10	8.77E-06	3.01E-03	0.0300	4.07E-08	1.26	2.84E-03	1.30E-10	6.31E-04	0.49	7.25E+05
0.25	0.387	0.00220	0.0055	0.0326	0.349	1.10	0.741	3.48E-10	6.70E-06	2.58E-03	0.0288	3.63E-08	1.26	3.02E-03	1.38E-10	6.68E-04	0.52	7.66E+05
0.28	0.388	0.00224	0.0056	0.0333	0.349	1.10	0.743	3.43E-10	6.59E-06	2.54E-03	0.0284	3.63E-08	1.26	3.09E-03	1.41E-10	6.83E-04	0.53	7.84E+05
Homogeneous solution																		
0.33	0.389	0.00226	0.0056	0.0336	0.349	1.10	0.744	4.18E-10	7.51E-06	2.70E-03	0.0281	3.89E-08	1.26	3.12E-03	1.42E-10	6.90E-04	0.54	7.92E+05
0.42	0.392	0.00234	0.0059	0.0351	0.351	1.10	0.748	4.05E-10	7.27E-06	2.62E-03	0.0272	3.89E-08	1.26	3.28E-03	1.49E-10	7.21E-04	0.57	8.27E+05
0.50	0.394	0.00241	0.0060	0.0362	0.352	1.10	0.752	3.96E-10	7.10E-06	2.56E-03	0.0266	3.89E-08	1.26	3.40E-03	1.54E-10	7.45E-04	0.59	8.55E+05
0.58	0.400	0.00256	0.0064	0.0390	0.354	1.10	0.761	3.26E-10	6.13E-06	2.31E-03	0.0252	3.72E-08	1.26	3.70E-03	1.66E-10	8.04E-04	0.64	9.23E+05
0.67	0.405	0.00270	0.0068	0.0415	0.357	1.10	0.768	3.11E-10	5.84E-06	2.20E-03	0.0240	3.72E-08	1.26	3.99E-03	1.77E-10	8.59E-04	0.69	9.86E+05
0.83	0.411	0.00288	0.0072	0.0447	0.359	1.10	0.777	2.39E-10	4.81E-06	1.94E-03	0.0227	3.47E-08	1.26	4.35E-03	1.92E-10	9.27E-04	0.75	1.06E+06
1.00	0.419	0.00312	0.0078	0.0492	0.362	1.10	0.789	2.23E-10	4.48E-06	1.81E-03	0.0211	3.47E-08	1.27	4.86E-03	2.11E-10	1.02E-03	0.84	1.17E+06
1.17	0.429	0.00341	0.0085	0.0548	0.366	1.10	0.803	2.20E-10	4.33E-06	1.71E-03	0.0195	3.55E-08	1.27	5.50E-03	2.36E-10	1.14E-03	0.95	1.31E+06
Inhomogeneous with precipitation as indicated by SAXS																		
1.33	0.380	0.00341	0.0085	0.0598	0.312	1.10	0.877	1.87E-10	3.69E-06	1.46E-03	0.0166	3.55E-08	1.27	6.56E-03	1.71E-10	8.27E-04	1.13	9.50E+05
1.50	0.387	0.00350	0.0088	0.0613	0.317	1.10	0.875	1.86E-10	3.65E-06	1.44E-03	0.0165	3.55E-08	1.27	6.71E-03	1.82E-10	8.80E-04	1.16	1.01E+06
1.67	0.377	0.00338	0.0084	0.0593	0.310	1.10	0.877	1.88E-10	3.70E-06	1.46E-03	0.0167	3.55E-08	1.27	6.50E-03	1.67E-10	8.11E-04	1.12	9.30E+05
1.83*	0.402	0.00370	0.0092	0.0645	0.328	1.10	0.872	1.82E-10	3.59E-06	1.42E-03	0.0162	3.55E-08	1.28	7.03E-03	2.06E-10	9.97E-04	1.21	1.14E+06
2.00	0.397	0.00363	0.0091	0.0634	0.325	1.10	0.873	1.83E-10	3.61E-06	1.42E-03	0.0163	3.55E-08	1.28	6.92E-03	1.98E-10	9.56E-04	1.19	1.10E+06
2.08	0.364	0.00320	0.0080	0.0564	0.299	1.10	0.880	1.92E-10	3.77E-06	1.49E-03	0.0170	3.55E-08	1.27	6.21E-03	1.48E-10	7.16E-04	1.07	8.22E+05
2.17	0.341	0.00293	0.0073	0.0518	0.282	1.10	0.885	1.98E-10	3.89E-06	1.54E-03	0.0175	3.55E-08	1.26	5.73E-03	1.21E-10	5.84E-04	0.99	6.70E+05
2.25	0.309	0.00254	0.0063	0.0452	0.258	1.10	0.891	2.08E-10	4.10E-06	1.62E-03	0.0185	3.55E-08	1.25	5.04E-03	8.70E-11	4.21E-04	0.87	4.83E+05
2.33	0.287	0.00228	0.0057	0.0408	0.240	1.10	0.896	3.51E-10	5.87E-06	1.97E-03	0.0192	4.17E-08	1.24	4.57E-03	6.80E-11	3.29E-04	0.79	3.78E+05
2.42	0.265	0.00203	0.0051	0.0365	0.223	1.10	0.900	3.66E-10	6.14E-06	2.06E-03	0.0200	4.17E-08	1.24	4.11E-03	5.23E-11	2.53E-04	0.71	2.91E+05
2.50	0.249	0.00186	0.0046	0.0335	0.211	1.10	0.903	3.79E-10	6.35E-06	2.13E-03	0.0207	4.17E-08	1.23	3.78E-03	4.28E-11	2.07E-04	0.65	2.38E+05
2.75	0.231	0.00165	0.0041	0.0299	0.197	1.10	0.907	3.96E-10	6.63E-06	2.23E-03	0.0216	4.17E-08	1.23	3.39E-03	3.30E-11	1.60E-04	0.59	1.83E+05
3.00	0.224	0.00158	0.0039	0.0287	0.191	1.10	0.908	4.03E-10	6.75E-06	2.27E-03	0.0220	4.17E-08	1.23	3.26E-03	2.98E-11	1.44E-04	0.56	1.66E+05
4.00	0.215	0.00148	0.0037	0.0270	0.184	1.10	0.910	4.42E-10	7.23E-06	2.37E-03	0.0225	4.27E-08	1.23	3.07E-03	2.59E-11	1.25E-04	0.53	1.44E+05
5.00	0.213	0.00147	0.0037	0.0268	0.183	1.10	0.910	4.44E-10	7.26E-06	2.38E-03	0.0226	4.27E-08	1.23	3.04E-03	2.54E-11	1.23E-04	0.52	1.41E+05

[a] Units are: Q ($CaLact_2$), M^3; Q (Ca_3Citr_2), M^5; $[Ca^{2+}] \times [CaCitr^-]^2$, M^4. Time value indicated by an asterisk is for maximal calcium ion activity in solution.

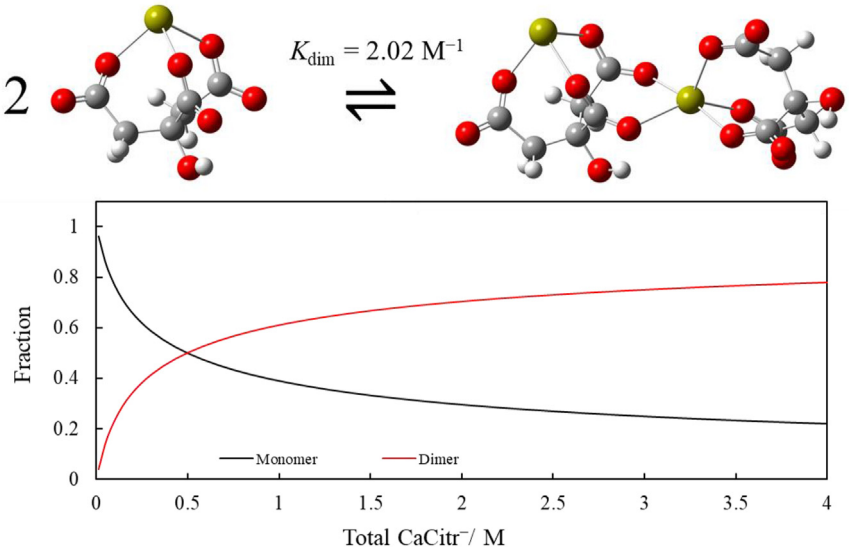

Fig. 4. The optimised structures (Ca in green, O in red, C in grey, H in white) and equilibrium concentrations of the dimer $Ca_2Citr_2^{2-}$ and the monomer of $CaCitr^-$ from the DFT calculation, see Table 4, for increasing total calcium citrate concentration at 25 °C. (For interpretation of the references to colour in this figure legend, the reader is referred to the Web version of this article.)

For all three temperatures, the calcium ion activity increases during dissolution as seen specifically for 25 °C from Table 2. Notably, the calcium ion activity continues to increase after all CLP has dissolved and during the period where the solution stays homogeneous and also after the end of the lag phase for precipitation. The increase in calcium ion activity after precipitation has started indicates that one or more ligand exchange reactions in the homogeneous solution must be slow in agreement with what was demonstrated for lactate/gluconate exchange at calcium in supersaturated calcium hydroxycarboxylate solutions during precipitation of calcium gluconate (Garcia, Hansen, Bailey, & Skibsted, 2020).

The slow ligand exchange could involve lactate dissociation from undissociated calcium lactate formed during dissolution:

$$CaLact_2 \cdot 5H_2O\ (s) \rightarrow CaLact_2\ (aq) + 5H_2O \quad (20)$$

$$CaLact_2\ (aq) \rightarrow CaLact^+ + Lact^- \quad (21)$$

$$CaLact^+ \rightarrow Ca^{2+} + Lact^- \quad (22)$$

prior to coordination of citrate:

$$Ca^{2+} + Citr^{3-} \rightarrow CaCitr^- \quad (23)$$

The rate of exchange of hydroxycarboxylate ligands at calcium (II) ions was previously based on hydrogen/deuterium isotope effects concluded to be controlled by a slow ligand dissociation. The present findings of a continuing increase in calcium ion activity in the supersaturated solutions following initiation of precipitation further supports this conclusion.

The speciation in the supersaturated solutions as shown for one example in Table 2 depends on the assumption of equilibrium among all dissolved species, which now can be concluded not to provide a full description. The conversion of calcium ion activity to calcium ion concentration is based on assumptions of values for the activity coefficients for the calcium ion in solutions with ionic strength around unity. In calcium chloride solutions of molarity around 0.33, the activity coefficients for calcium chloride are not sensitive to small variations in ionic strength (Robinson & Stokes, 1959). The results of calculations for speciation using the value $\gamma_{Ca}^{2+} = 0.4$ for the activity coefficient for Ca^{2+} gave consistent results, as the sum of all calcium species was in agreement with the total calcium concentration as calculated from the added amount of CLP. The calculated speciation is accordingly in agreement with the total calcium concentration validating our method of calculation and the used activity coefficient for calcium.

In the concentrated solutions formation of other species may need to be taken into account. The dimerisation reaction,

$$2CaCitr^- \rightleftharpoons Ca_2Citr_2^{2-},\ K_{dim} = 2.02\ \text{M}^{-1} \quad (24)$$

finds some support from quantum mechanical calculations using the Density Functional Theory (DFT) method as seen in Fig. 4, which gives the value $K_{dim} = 2.02$ M^{-1}.

Based on the speciation for the solution with critical conditions at 25 °C, the time development for each species is shown in Fig. 5A. The ion product determining the driving force for precipitation

$$Q = [Ca^{2+}]^3 \cdot [Citr^{3-}]^2 \quad (25)$$

shows a slow increase up to 2 h, which was the lag phase for initiation of precipitation and followed by a rapid decay during precipitation. The ratio between the ion product and the solubility product Q/K_{sp} is a measure of the degree of supersaturation. Using the value $K_{sp} = 1.8 \times 10^{-16}$ M^5 for $Ca_3Citr_2 \cdot 6H_2O$ and value $K_{sp} = 5.8 \times 10^{-3}$ M^3 for $CaLact_2 \cdot 5H_2O$ as previously determined for unity ionic strengths (Vavrusova, Munk, & Skibsted, 2013; Vavrusova & Skibsted, 2016), it may be seen from Table 2 that

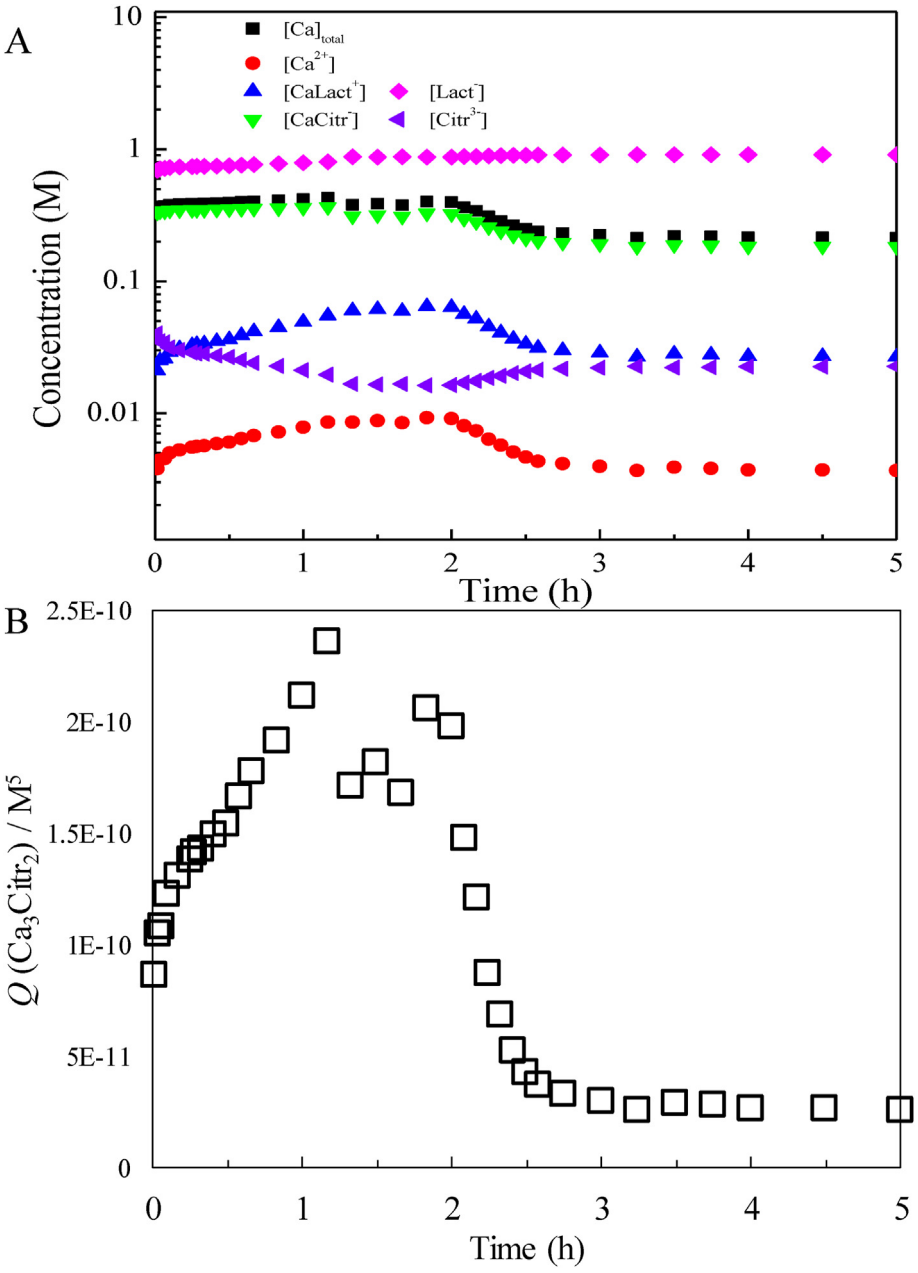

Fig. 5. (A) Change in concentration of dominating species during the codissolution, metastable supersaturation and precipitation for $CaLact_2 \cdot 5H_2O$ (0.519 mol) and $Na_3Citr \cdot 2H_2O$ (0.408 mol) in 1000 mL of water based on electrochemical measurement at 25 °C. (B) $Q = [Ca^{2+}]^3[Citr^{3-}]^2$ was calculated as a measure of driving force for precipitation during the three stages at 25 °C.

although this ratio decreases during precipitation, the ratios still have a value far above unity also when correcting for precipitation of calcium citrate with time. Inclusion of the dimer calcium citrate complex into calculation reduces the value of Q/K_{sp} in support of the importance of this dimerisation in concentrated solutions. However, an important conclusion seems to be that the solutions do not equilibrate fully during the time period considered or that polymers of calcium citrate may be involved. It should be noted, that a similar conclusion was reached, when the Q/K_{sp} ratio based on activity was considered.

The Boltzmann function (Eq. (26)) was used to account for the intensity/time curves from SAXS measurements during precipitation following the lag phase (*LP*, in h) and for estimating the rate constant (k_B, in h^{-1}) for the precipitation phase as seen in Fig. 6A and B (Liu et al., 2018). Here Int_0 and Int_{end} are the initial and the final levels of intensity (*Int*), t_m is the time (t) of middle point with the middle point of intensity Int_m equals to $(Int_0 + Int_{end})/2$:

$$Int(t) = \frac{Int_0 - Int_{end}}{1 + e^{(t-t_m)/P_m}} + Int_{end} \quad (26)$$

The slope of middle point k_m was the reaction rate used for estimating k_B (Ossorio et al., 2017) and calculated from Eq. (27), where $4P_m$ is the length of the precipitation phase:

$$k_m = \frac{Int_{end} - Int_0}{4P_m} \quad (27)$$

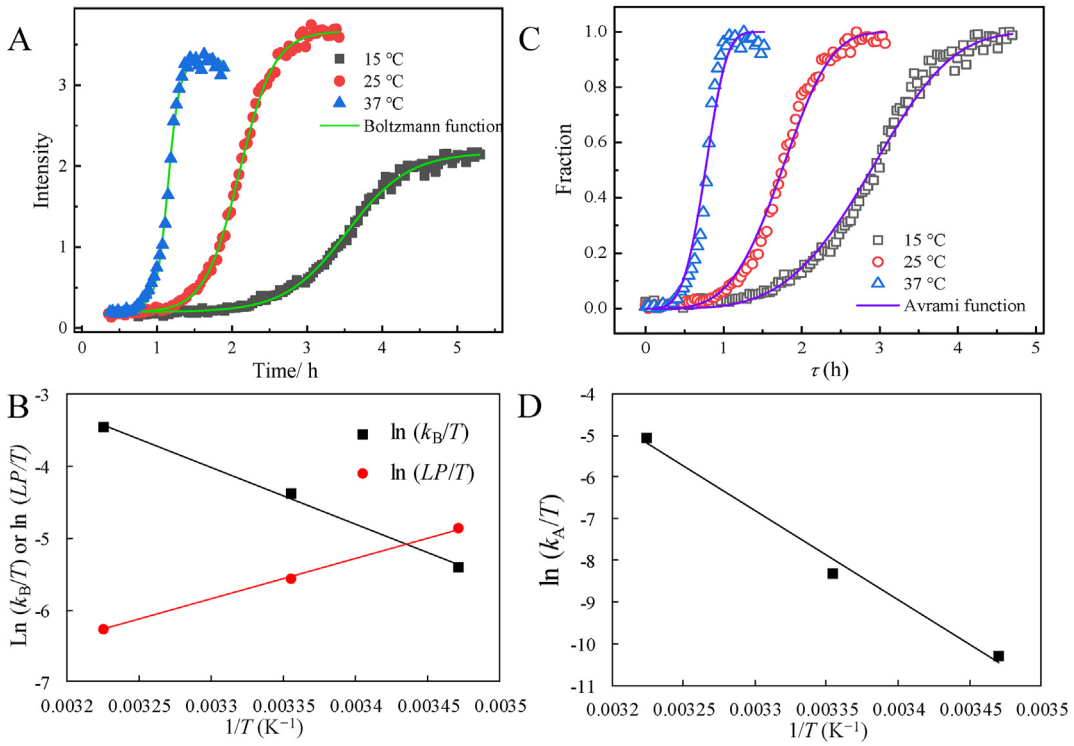

Fig. 6. Scattering intensity from SAXS measurements during precipitation of $Ca_3Citr_2 \cdot 6H_2O$ at 15, 25, and 37 °C from supersaturated solutions formed during codissolution of $CaLact_2 \cdot 5H_2O$ (0.519 mol) and $Na_3Citr \cdot 2H_2O$ (0.408 mol) in 1000 mL water analyzed according to the Boltzmann function (A) and analysed according to the Avrami function (C) for estimating the lag phase (*LP*), and the rate constant (k_B or k_A) according to Eqs. (26), (27) and (29). (B) *LP* and k_B from the Boltzmann function further analyzed according to the Eyring equation of Eq. (28) to yield an enthalpy of activation of 65.6 ± 3.4 kJ mol^{-1} and − 47.4 ± 1.6 kJ mol^{-1} for the rate constant for precipitation and the lag phase, respectively. (D) The k_A estimated according to the Avrami equation gave an enthalpy of activation of 177 ± 20 kJ mol^{-1}.

The values of *LP* can be derived by solving the equations of $Int(t) - Int_m = (Int)'_m\,(t - t_m)$ and $Int(t) = Int_0$, which is the tangent line at the middle point and the initial baseline. The experimental results were well described by the Boltzmann model ($R^2 > 0.99$), and the *LP* and k_B ($\approx k_m$) gave an activation enthalpy of −47.4 kJ mol^{-1} and 65.6 kJ mol^{-1} according to the Eyring equation (Eq. (28)) for the lag phase and the rate of precipitation, respectively, as shown in Fig. 6B and Table 1:

$$\ln k/T = -\Delta H^{\#}/R \cdot 1/T + \ln \kappa \cdot b/h + \Delta S^{\#}/R \quad (28)$$

where, $\Delta H^{\#}$, κ, b, and $\Delta S^{\#}$ are enthalpy of activation, transmission coefficient assumed to unity, the Boltzmann constant, and entropy of activation, respectively.

The normalised SAXS results could be described by Avrami model for precipitation reactions according to equation (Eq. (29)) as shown in Fig. 6C and D, where *Deg* is the degree of crystallisation from the normalised intensity, τ is the time elapsed after the supersaturation phase, k_A is the Avrami constant which is related to the rate constant of crystallisation, and n is Avrami exponent characteristic for the crystal growth type (Erukhimovitch & Baram, 1995; Sun, Liu, & Lu, 1996).

$$Deg = 1 - \exp\left[-(-k_A \cdot \tau)^n\right] \quad (29)$$

With a fixed $n = 4$, the curves were found to match well ($R^2 > 0.98$) at each temperature, which indicates that crystal nucleation and growth can be accounted for by a three-dimensional spherical growth as seen in Fig. 6C. The temperature dependence of k_A against temperature curves gave an enthalpy of activation of 177.3 kJ mol^{-1} according to the Eyring equation (Eq. (28)), as seen in Fig. 6D and Table 1. The activation parameters could be estimated both from the rate parameters obtained by the Boltzmann and the Avrami equations. The activation parameters obtained from the Avrami equation seems more reliable as they are derived from the normalised data.

The $a(Ca^{2+})$ dynamics were followed during dissolution and precipitation to provide a mechanistic understanding of the supersaturation phenomena as shown in Fig. 7. The rate of unassisted dissolution of CLP depends moderately on temperature and $a(Ca^{2+}$, 37 °C) > $a(Ca^{2+}$, 25 °C) > $a(Ca^{2+}$, 15 °C) as seen in Fig. 7A for the dissolution of CLP (0.519 mol in 1000 mL) with an activation enthalpy of 56 kJ mol^{-1} as shown in Fig. 7A,D and Table 3. The critical conditions for each of the temperature for 0.519 mol CLP were found to be 0.544, 0.408, and 0.204 mol NCD dissolved in 1000 mL of water, respectively, at 15, 25, and 37 °C. The temperature effect for the citrate assisted dissolution corresponding to the critical conditions had the larger activation enthalpy of 115 kJ mol^{-1}. Decrease in calcium activity as measured electrochemically due to precipitation showed less dependence on temperature with an enthalpy of 28 kJ mol^{-1}, see Fig. 7B,E and Table 3. For the reaction conditions of 0.519 mol CLP and 0.544 mol NCD in 1000 mL water corresponding to the critical condition at 25 °C, the temperature had a similar effect for both the increase and decrease

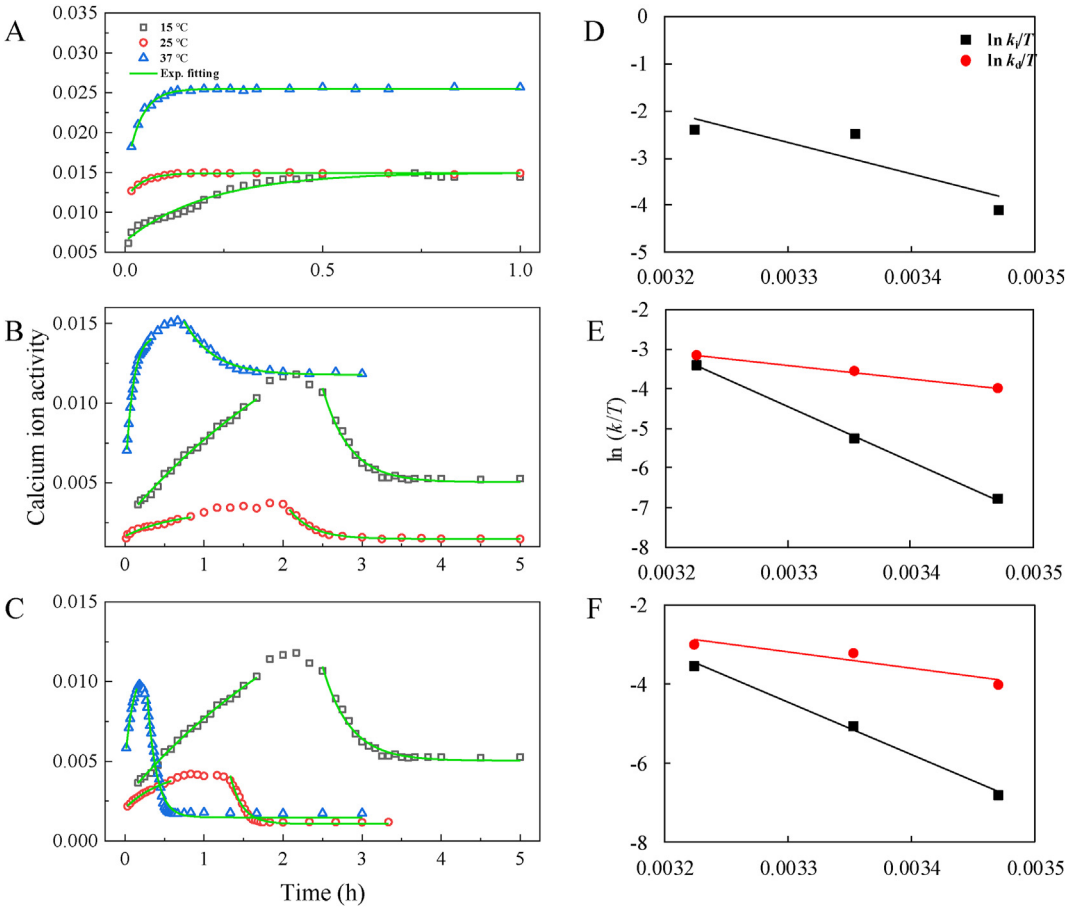

Fig. 7. Calcium ion activities $a(Ca^{2+})$ during dissolution of $CaLact_2 \cdot 5H_2O$ in water, during codissolution of $CaLact_2 \cdot 5H_2O$ and $Na_3Citr \cdot 2H_2O$ in water, and during precipitation from the resulting spontaneously supersaturated solution of $Ca_3Citr_2 \cdot 6H_2O$ at 15, 25, and 37 °C. (A) Dissolution of $CaLact_2 \cdot 5H_2O$ (0.519 mol) in 1000 mL water, (B) dissolution of $CaLact_2 \cdot 5H_2O$ (0.519 mol) + $Na_3Citr \cdot 2H_2O$ (critical amount according to Fig. 1) in 1000 mL water, (C) dissolution of for $CaLact_2 \cdot 5H_2O$ (0.519 mol) + $Na_3Citr \cdot 2H_2O$ (0.544 mol) in 1000 mL water at 15, 25, 37 °C. The increasing and decreasing phases for calcium ion activity were each described by exponential functions and the rate constants estimated were used to calculate the activation parameters using Eyring equation. (D) (E) (F) are for (A) (B) (C), respectively, see Table 3.

Table 3
Rate constant for dissolution of calcium lactate (0.519 mol) in 1000 mL water in absence (k_i) or presence (k_i) of critical amount of sodium citrate as required for critical spontaneous supersaturation or in presence (k_i) of 0.544 mol of sodium citrate, together with rate constant for precipitation (k_d) of calcium citrate at 15, 25 or 37 °C, and activation parameters from Eyring equation for both processes from electrochemical measurement of calcium ion activity.[a]

CLP/NCD (mol in 1000 mL water)	Rate constant	15 °C	25 °C	37 °C	$\Delta H^{\#}$ (kJ mol^{-1})	$\Delta S\#$ (J mol^{-1} K^{-1})
0.519	k_i (h^{-1})	4.7 ± 0.4	24.9 ± 1.4	27.6 ± 1.2	56 ± 29	−35 ± 18
0.519/critical amount	k_i (L mol^{-1} h^{-1})	0.3 ± 0.1	1.5 ± 0.7	10.3 ± 0.3	115 ± 3	143 ± 4
	k_d (L mol^{-1} h^{-1})	5.4 ± 0.4	8.5 ± 0.3	13.0 ± 0.2	28 ± 2	−135 ± 9
0.519/0.544	k_i (L mol^{-1} h^{-1})	0.3 ± 0.1	1.9 ± 0.2	9.0 ± 1.2	110 ± 9	127 ± 11
	k_d (L mol^{-1} h^{-1})	5.4 ± 0.4	11.9 ± 1.1	15.2 ± 1.1	33 ± 11	−114 ± 38

[a] Abbreviations are: CLP, calcium lactate ($CaLact_2 \cdot 5H_2O$); NCD, sodium citrate ($Na_3Citr \cdot 2H_2O$). Calcium citrate: $Ca_3Citr_2 \cdot 6H_2O$. The critical amounts for NCD are 0.544, 0.408, and 0.204 mol at 15, 25, and 37 °C, respectively.

in Ca^{2+} activity with activation enthalpies of 110 and 33 kJ mol^{-1}, respectively, see Fig. 7C,F and Table 3.

The precipitates collected in the SAXS experiments investigating the rate of precipitation from the supersaturated solution with a calcium/citrate ratio of 0.519/0.544, had DSC thermograms comparable with thermograms of calcium citrate hexahydrate (CCH) standards confirming that calcium citrate precipitating for conditions with $Ca^{2+}/Citr^{3-} < 3/2$ is the hexahydrate, see Fig. 8 (Liu et al., 2021).

Table 4
Thermodynamic parameters for the formation of dimeric calcium citrate from DFT calculation.[a]

Parameter	Value
ΔH^0_{dim}	−49.0 kJ mol^{-1}
ΔG^0_{dim}	−1.75 kJ mol^{-1}
ΔS^0_{dim}	−159 J mol^{-1} K^{-1}

[a] $K_{dim} = 2.02$ L mol^{-1}, calculated from $\Delta G^0_{dim} = -RT \ln K_{dim}$ for 25 °C.

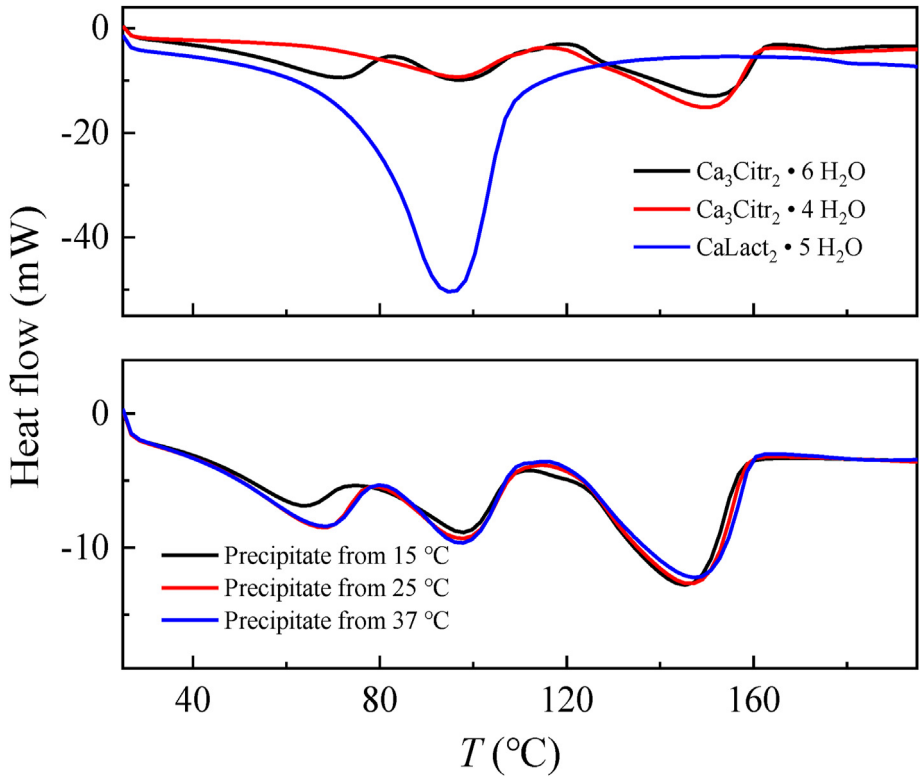

Fig. 8. Differential scanning calorimeter thermograms of dried precipitates from experiments with SAXS measurements and standards of $Ca_3Citr_2 \cdot 6H_2O$, $Ca_3Citr_2 \cdot 4H_2O$, and $CaLact_2 \cdot 5H_2O$.

4. Discussion

Calcium lactate pentahydrate has a moderate solubility in water at ambient conditions, which, however, is strongly enhanced by the presence of citrate or of other hydroxycarboxylates (Vavrusova et al., 2017). The increase in aqueous solubility may only partly be explained by complex binding of calcium by citrate, since hydrates of calcium citrate are only of low solubility in water and are expected to precipitate. The rate of precipitation of calcium citrate is slow, and the solution resulting from codissolution of calcium lactate and sodium citrate is strongly supersaturated. This spontaneous supersaturation is rather robust as the supersaturation may persist for hours and even days (Vavrusova et al., 2017).

The degree and robustness of the spontaneous supersaturation depend on the difference in rate of citrate assisted dissolution of calcium lactate and rate of precipitation of calcium by citrate. Both reactions involve complex formation of calcium by citrate and a key to the understanding of the persistence of the supersaturation is the rate of ligand exchange during the transformation of the calcium lactate complex to the calcium citrate complex.

Exchange of hydroxycarboxylates ligands at calcium (II) centers was recently found slow for aqueous supersaturated solutions of high viscosity and the exchange reaction could for gluconate/lactate exchange be characterised by a half-life of 5 h (Garcia et al., 2020). For a more detailed discussion of the spontaneous supersaturation, the over-all process will be divided into three phases: (I) a dissolution phase, where calcium ion activity increases as more solid CLP dissolves into the homogeneous fraction of the suspension, followed by (II) a metastable supersaturation phase, where calcium ion activity continues to increase in the homogeneous solution of constant total calcium concentration, and followed by (III) a precipitation phase, where calcium ion activity decreases as calcium citrate hexahydrate continuous to precipitate and the total calcium concentration decreases.

The calcium ion activity increase during the dissolution phase is in agreement with the increase in total dissolved calcium salts. This is evident for the speciation based on measurement of calcium ion activity and shown in Table 2 for critical supersaturation conditions at 25 °C. The continuing increase in calcium ion activity in phase II with a constant total calcium concentration can only be explained by a slow redistribution among dissolved calcium species in a process which finds a parallel in calcium redistribution in milk during cooling (Gaucheron, 2005). Calcium ion activity increases during the aging of the homogeneous supersaturated solution in agreement with a slow dissociation of calcium ions from initially dissolved calcium complexes of lactate, see Eqs. (21) and (22). The precipitation of calcium citrate seems to depend on coordination of citrate to calcium in agreement with the reaction of Eq. (23). The binding of lactate to calcium is weak with $K = 8\ \text{M}^{-1}$ compared with binding of citrate to calcium with $K = 2400\ \text{M}^{-1}$, and the formation of the calcium citrate complex according to the reaction of Eq. (23) from free calcium ions is the first step towards precipitation according to the reaction

$$Ca^{2+} + 2CaCitr^{-} \rightarrow Ca_3Citr_2 \tag{30}$$

The relative driving force for precipitation, Q, as calculated from Eq. (25) is in Fig. 5 seems to increase in a non-linear fashion for up to 2 h for the experiment at 25 °C for which speciation is shown in Table 2. Precipitation is already initiated shortly after 1 h of equilibration, and while the driving force may be calculated as Q from Eq. (25), any kinetic barriers are more difficult to identify. The binding of calcium to citrate, the reaction of Eq. (23) may not be rate determining for formation of intermediates leading to

crystallisation. The dimer formed in the reaction of Eq. (24) may rather be rate determining for the crystallisation reaction

$$Ca^{2+} + Ca_2Citr_2^{2-} \rightarrow Ca_3Citr_2\,(aq) \rightarrow Ca_3Citr_2\,(s) \quad (31)$$

The enthalpy of activation of 60 kJ mol^{-1} determined from SAXS experiment using the Boltzmann function, may refer to the last step in the reaction sequence of Eq. (31) as rate determining, since it depends on detection of a solid. The lower enthalpy of activation of around 30 kJ mol^{-1} may in contrast refer to the reaction of Eq. (24) or to the first step in the reaction of Eq. (27), as it depends on measurement of calcium ion activity in solution. The negative entropy of activation further supports this conclusion as these reactions both decrease the number of ions.

The different crystallisation types of calcium lactate pentahydrate and calcium citrate hexahydrate may enhance the observed supersaturation phenomena. CLP formation is a one-dimensional process (Lee, Lee, & Kim, 2013), but the formation of CCH is a three-dimensional process according to the analysis by the Avrami equation. During the dissolution process the presence of CLP solids as a nucleus for crystallisation will not easily induce the growth of CCH, and the CLP + NCD system needs to go through supersaturation for crystallisation.

5. Conclusion

The supersaturated solutions formed by codissolution of CLP and NCD only slowly approach equilibrium. Following dissolution of CLP, the supersaturated solution is in equilibrium with respect to precipitation of CLP, but clearly not with respect to precipitation of CCH. Q as calculated from Eq. (25) for CCH and a similar calculation for CLP indicate this difference. For calcium citrate the strong deviation from equilibrium may be due to polymerisation reaction as is indicated for the calcium citrate dimer. Independent of the degree of polymerisation of calcium citrate in supersaturated solutions, the spontaneous supersaturation may be important for calcium bioavailability and deserves more attention in relation to human nutrition and the uniqueness of milk as a vehicle for calcium and also for formulation of functional foods.

Declaration of competing interest

The authors declare that they have no known competing financial interests or personal relationships that could have appeared to influence the work reported in this paper.

Acknowledgements

The authors acknowledge the support from China Scholarship Council (CSC, No. 201806360266) and from the Innovation Fund Denmark/FAPESP project - Novel Aging - Technologies and solutions to manufacture novel dairy products for healthy aging. We thank Martin Schmiele from Niels Bohr Institute for his help on SAXS setting up and measurement.

References

Apelblat, A., & Barthel, J. (1991). Conductance studies on aqueous citric-acid. *Zeitschrift Fur Naturforschung Section a-a Journal of Physical Sciences, 46*, 131–140.

Bijl, E., Huppertz, T., van Valenberg, H., & Holt, C. (2019). A quantitative model of the bovine casein micelle: Ion equilibria and calcium phosphate sequestration by individual caseins in bovine milk. *European Biophysics Journal, 48*, 45–59.

Chatterjee, K. P., & Dhar, N. R. (1924). Studies of sparingly soluble salts, readily obtained from hot solutions of reacting substances I. *Journal of Physical Chemistry, 28*, 1009–1028.

Cheng, H., Garcia, A. C., Tang, N., Danielsen, B. P., & Skibsted, L. H. (2018). Combinations of isocitrate and citrate enhance calcium salt solubility and supersaturation robustness. *International Dairy Journal, 85*, 225–236.

Davies, W. C. (1962). *Ion association*. Washington, DC, USA: Butterworths.

Erukhimovitch, V., & Baram, J. (1995). Nucleation and growth transformation kinetics. *Physical Review B, 51*, 6221–6230.

Frisch, M. J., Trucks, G. W., Schlegel, H. B., Scuseria, G. E., Robb, M. A., Cheeseman, J. R., et al. (2009). *Gaussian 09, revision C.01*. Wallingford, CT, USA: Gaussian, Inc.

Garcia, A. C., Hansen, J. S., Bailey, N., & Skibsted, L. H. (2020). Slow lactate gluconate exchange in calcium complexes during precipitation from supersaturated aqueous solutions. *Food Research International, 137*, Article 109539.

Gaucheron, F. (2005). The minerals of milk. *Reproduction Nutrition Development, 45*, 473–483.

Gueguen, L., & Pointillart, A. (2000). The bioavailability of dietary calcium. *Journal of the American College of Nutrition, 19*, 119S–136S.

Hartley, A., Paternoster, L., Evans, D. M., Fraser, W. D., Tang, J., Lawlor, D. A., et al. (2020). Metabolomics analysis in adults with high bone mass identifies a relationship between bone resorption and circulating citrate which replicates in the general population. *Clinical Endocrinology, 92*, 29–37.

Holt, C. (2013). Unfolded phosphopolypeptides enable soft and hard tissues to coexist in the same organism with relative ease. *Current Opinions in Structural Biology, 23*, 420–425.

Holt, C., Lenton, S., Nylander, T., Sorensen, E. S., & Teixeira, S. C. M. (2014). Mineralisation of soft and hard tissues and the stability of biofluids. *Journal of Structural Biology, 185*, 383–396.

Holt, C., Sorensen, E. S., & Clegg, R. A. (2009). Role of calcium phosphate nanoclusters in the control of calcification. *FEBS Journal, 276*, 2308–2323.

Kaduk, J. A. (2018). Crystal structures of tricalcium citrates. *Powder Diffraction, 33*, 98–107.

Kubantseva, N., & Hartel, R. W. (2002). Solubility of calcium lactate in aqueous solution. *Food Reviews International, 18*, 135–149.

Lee, S., Lee, C. H., & Kim, W. S. (2013). Taylor vortex effect on flocculation of hairy crystals of calcium lactate in anti-solvent crystallization. *Journal of Crystal Growth, 373*, 32–37.

Liu, X. C., Du, H. H., Fu, L. M., Han, R. M., Wang, P., Ai, X. C., et al. (2018). Integrity of membrane structures in giant unilamellar vesicles as assay for antioxidants and prooxidants. *Analytical Chemistry, 90*, 2126–2133.

Liu, X. C., Kirkensgaard, J. J. K., & Skibsted, L. H. (2021). Hydrates of calcium citrate and their interconversion in relation to calcium bioaccessibility. *Food Research International, 2021*, Article 109867.

Li, M., Wang, L., & Putnis, C. V. (2017). Energetic basis for inhibition of calcium phosphate biomineralization by osteopontin. *Journal of Physical Chemistry B, 121*, 5968–5976.

Ossorio, M., Stawski, T. M., Rodriguez-Blanco, J. D., Sleutel, M., Garcia-Ruiz, J. M., Benning, L. G., et al. (2017). Physicochemical and additive controls on the multistep precipitation pathway of gypsum. *Minerals, 7*, Article 140.

Pak, C. Y., Harvey, J. A., & Hsu, M. C. (1987). Enhanced calcium bioavailability from a solubilized form of calcium citrate. *Journal of Clinical Endocrinology & Metabolism, 65*, 801–805.

Quarto, M., Nitride, C., Ferranti, P., Mauriello, R., Garro, G., Di Stasio, M., et al. (2018). Peptidomic study on in vitro and in vivo phosphopeptide release during the chewing of gum fortified with a commercial casein hydrolysate. *International Dairy Journal, 79*, 78–84.

Righellato, E. C., & Davies, C. W. (1930). The extent of dissociation of salts in water. Part II. Uni-bivalent salts. *Transactions of the Faraday Society, 26*, 592–599.

Robinson, R. A., & Stokes, R. H. (1959). *Electrolyte solutions* (2nd ed.). London, UK: Butterworths.

Sun, N. X., Liu, X. D., & Lu, K. (1996). An explanation to the anomalous Avrami exponent. *Scripta Materialia, 34*, 1201–1207.

Vavrusova, M., Danielsen, B. P., Garcia, A. C., & Skibsted, L. H. (2018). Codissolution of calcium hydrogenphosphate and sodium hydrogencitrate in water. Spontaneous supersaturation of calcium citrate increasing calcium bioavailability. *Journal of Food and Drug Analysis, 26*, 330–336.

Vavrusova, M., Garcia, A. C., Danielsen, B. P., & Skibsted, L. H. (2017). Spontaneous supersaturation of calcium citrate from simultaneous isothermal dissolution of sodium citrate and sparingly soluble calcium hydroxycarboxylates in water. *RSC Advances, 7*, 3078–3088.

Vavrusova, M., Liang, R., & Skibsted, L. H. (2014). Thermodynamics of dissolution of calcium hydroxycarboxylates in water. *Journal of Agricultural and Food Chemistry, 62*, 5675–5681.

Vavrusova, M., Munk, M. B., & Skibsted, L. H. (2013). Aqueous solubility of calcium l-lactate, calcium d-gluconate, and calcium d-lactobionate: Importance of complex formation for solubility increase by hydroxycarboxylate mixtures. *Journal of Agricultural and Food Chemistry, 61*, 8207–8214.

Vavrusova, M., & Skibsted, L. H. (2016). Aqueous solubility of calcium citrate and interconversion between the tetrahydrate and the hexahydrate as a balance between endothermic dissolution and exothermic complex formation. *International Dairy Journal, 57*, 20–28.

Wang, Q., & Ma, Y. (2020). Effect of temperature and pH on salts equilibria and calcium phosphate in bovine milk. *International Dairy Journal, 110*, Article 104713.

Wang, Z., Ma, G., & Liu, X. Y. (2009). Will fluoride toughen or weaken our teeth? Understandings based on nucleation, morphology, and structural assembly. *Journal of Physical Chemistry B, 113*, 16393–16399.

Wang, L. M., Wang, W., Li, X. C., Peng, L., Lin, Z. Q., & Xv, H. Z. (2012). Calcium citrate: A new biomaterial that can enhance bone formation in situ. *Chinese Journal of Traumatology, 15*, 291–296.

Zhou, Y., Xue, S., & Yang, J. J. (2013). Calciomics: Integrative studies of Ca^{2+}-binding proteins and their interactomes in biological systems. *Metallomics, 5*, 29–42.